THE JOURNAL OF PHYSICAL CHEMISTRY C

ARTICLE

pubs.acs.org/JPCC

Modifying an Infrared Microscope To Characterize Propagating Surface Plasmon Polariton-Mediated Resonances

Marvin A. Malone, Katherine E. Cilwa, Matthew McCormack, and James V. Coe*

Department of Chemistry, 100 West 18th Avenue, The Ohio State University, Columbus, Ohio 43210-1173, United States

ABSTRACT: Metal films with periodic arrays of subwavelength holes (meshes) show extraordinary transmission resonances using ordinary, benchtop Fourier transform infrared (FTIR) spectrometers. However, the infrared study of single, wavelength-scale particles with an FTIR microscope typically involves an instrument with a large range of angles that will disperse surface plasmon polariton (SPP) resonances. This work shows how to add an aperture and mesh to a commercial FTIR microscope system to obtain well-defined and identifiable SPP transmission-mediated resonances using a dispersion geometry that is convenient to a microscope, that is, rotation of the mesh in the focal plane of the microscope about the microscope's optical axis. Momentum matching equations are derived that identify the resonances and model the measured dispersion of each resonance. These equations effectively model the data and cover the parts of momentum space that fall between better-known, high symmetry geometric arrangements, which are often called ΓX and ΓM in the reciprocal space of a square lattice. Both a region of extensive overlapping of many resonances and a very narrow and isolated resonance were discovered that may be particularly useful for SPP studies.

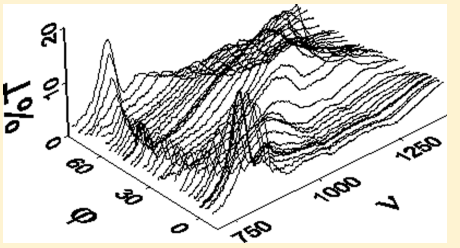

INTRODUCTION

We have been developing techniques to apply propagating surface plasmon polariton (SPP) resonances to the spectroscopic study of individual, subwavelength-sized particles. SPPs, mixed states of light and conducting electrons at the surface of a patterned metal surface, are part of, that is, mediate, the extraordinary transmission/reflection resonances of patterned metal meshes. A fair body of work has been presented by us showing that plasmonic metal mesh is a very useful substrate for sensing resonance shifts and for infrared (IR) absorption studies for both benchtop[1−10] and microscope[11−13] studies. Dispersion studies[14−19] reveal much about the plasmonic nature of two-dimensional periodic mesh, which has been a subject of several reviews[10,20,21] (to name only a few).

Our plasmonic mesh is a freestanding nickel film with square holes (5 μm width), in a square lattice (L = 12.6 μm lattice parameter), with a thickness of ∼2 μm as shown in Figure 1a. Transmission spectra of the same piece of Ni mesh obtained with a Fourier transform infrared (FTIR) microscope as compared to a benchtop FTIR instrument are shown in Figure 1b. There are considerable differences: (i) the primary resonance at 752 cm^{-1} of the benchtop spectrum does not occur in the FTIR microscope spectrum, (ii) the FTIR microscope trace has two broad resonances at higher wavenumbers, and (iii) the FTIR microscope trace has much more transmission at the higher wavenumbers. The FTIR microscope spectrum of mesh has no predominant and assigned plasmonic resonance, which may be good for spectroscopy in an FTIR microscope, but is bad for sensing the shift of resonances.

These differences can be understood by noting that the optical geometry in the sample region of a FTIR microscope system is significantly different from that of a typical benchtop FTIR system. Our IR microscope (Perkin-Elmer Spotlight 300) employs a pair of Cassegrain optics (reflective mirror combinations), which share a focal point at the sample. They only transmit rays from 17° to 37° off of the optical axis; that is, a ring of light is focused onto and collected from the sample. In contrast, a desktop FTIR system has a beam that is perpendicular to the sample (an average angle of 0° relative to the optical axis with a Gaussian standard deviation of a few degrees about that average). A resonance at each angle in the large range of angles of an FTIR microscope will be dispersed differently, producing a smearing out of plasmonic resonances, instead of well-defined resonances. Also, the range of large off axis angles enables higher order diffraction spots to be collected, which would be lost in a zero order benchtop FTIR transmission spectrum, which manifests as greater transmission at higher wavenumbers.

In this work, we describe how to add an aperture between the lower optics and the input of the sample, which greatly reduces the spread of angles narrowing transmission resonances. In a microscope, the mesh must be oriented perpendicular to the optical axis to keep the mesh in focus, so the natural coordinate for dispersion is rotation of the mesh within the focal plane about the microscope's optical axis. A geometric arrangement between the aperture and mesh is described, which enables the production and identification of much sharper propagating SPP transmission resonances. This system has enabled a dispersion study with a Cassegrain microscope system by rotation of mesh rather than the tilting of mesh previously employed with a benchtop FTIR system.[19]

Received: February 7, 2011
Revised: April 28, 2011
Published: June 06, 2011

IR MICROSCOPE GEOMETRY AND φ DISPERSION

A piece of mesh in a Cassegrain optical microscope system with an aperture is shown in Figure 2 where the mesh is held parallel to the ground and perpendicular to the microscope's optical axis. Reflective optics block light from traveling perpendicular to the mesh; only angles from 17° to 37° relative to the system's optical axis are allowed to pass. The mesh is stretched tightly over a 3.2 mm hole in an aluminum slide, so the substrate for the mesh is air; that is, it is freestanding. The mesh is placed at the focal plane of the cones of the microscope's infrared light defining the focus as the origin of the coordinate system. The center of an off-axis aperture (~24.0 mm below the mesh, 13.84 mm off the optical axis, with a 2.38 mm diameter) defines a new axis, the z-axis, for detectable light. Let the angles of rotation about the x-axis be γ, the y-axis be θ, and the z-axis be φ . If the y-axis is set within the mesh and aligned with the holes, then the orientation of the mesh (parallel to the ground with a vertical system) is defined by $\gamma = 0$ and a fixed and nonzero value of $\theta = \theta_0 = \sim 28°$. This leaves the natural dispersion coordinate as rotation about the microscope axis to change φ (rotation about the z-axis) at a fixed tilt value of θ_0 (about the y-axis). Using the concept of momentum matching, the square of the momentum of light in the effective film defined by the mesh [left side of eq 1] can be equated to the momentum components due to light ($k_x = 2\pi\tilde{\nu}$ sin θ_0 cos φ and $k_y = 2\pi\tilde{\nu}$ sin θ_0 sin φ)[22] and the grating ($2\pi i/L$ along x and $2\pi j/L$ along y) as

$$(2\pi\tilde{\nu}n_{\text{eff}})^2 = \left(k_x + \frac{2\pi i}{L}\right)^2 + \left(k_y + \frac{2\pi j}{L}\right)^2 \qquad (1)$$

where L is the lattice parameter, $\tilde{\nu}$ is the wavenumber or reciprocal of wavelength, n_{eff} is the real part of the effective index of refraction of the effective film with subwavelength features (note that it could have a weak dependence with wavelength, but we have modeled our data using a constant value), and i and j are integer indices (positive, negative, or zero), which will identify each resonance. Making substitutions and solving for $\tilde{\nu}$ gives dispersion as a function of the φ coordinate given a fixed tilt of θ_0.

$$\tilde{\nu}_{i,j}(\varphi) = \frac{\frac{\sin\theta_0}{L}(i\cos\varphi + j\sin\varphi) \pm \sqrt{\left[\frac{\sin\theta_0}{L}(i\cos\varphi + j\sin\varphi)\right]^2 + [n_{\text{eff}}^2 - (\sin\theta_0)^2]\left(\frac{i^2+j^2}{L^2}\right)}}{[n_{\text{eff}}^2 - (\sin\theta_0)^2]} \qquad (2)$$

This expression will be used to model dispersion and label the resonances. It is very useful as it serves to connect dispersion at a fixed tilt angle, θ_0, in ΓX space to that in ΓM space (the high symmetry arrangements in reciprocal space).

EXPERIMENTAL SECTION

A Perkin-Elmer Spotlight 300 FTIR microscope system was modified with a 2.38 mm diameter aperture. It was placed 13.84 mm off of the optical axis of the instrument and at ~24.0 mm below the focal plane in which the mesh or sample sits. Using unpolarized light and a background without mesh, 32 different IR transmission spectra of Ni mesh (geometry given in first paragraph of the Introduction) were recorded at values of φ (see Figure 2 for the definition of rotation within the focal plane about the microscope axis) varying from −6.9° to 77.7°. Each spectrum spans a wavenumber range of 650−4000 cm^{-1}, at a resolution of 4 cm^{-1}, with 100 scans, and requiring about 2.5 min. The spectra are plotted together in Figure 3. The angles were measured using microscope images of the mesh and the angle of the holes relative to the horizontal axis. Note the differences of these spectra from the microscope spectrum without an aperture in Figure 1b (top). The resonances are much narrower and shift in systematic ways with changes in rotation; that is, they disperse.

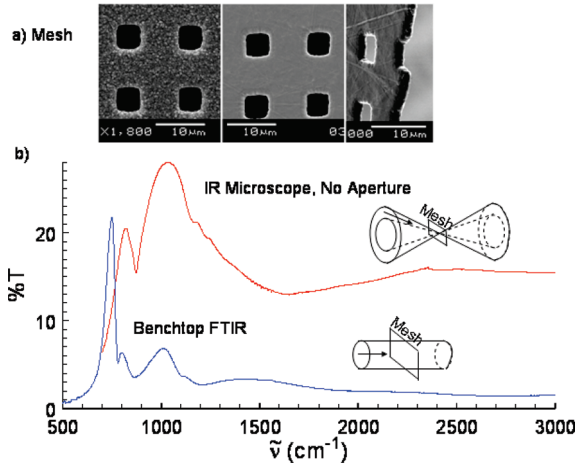

Figure 1. (a) Scanning electron microscope image of plasmonic Ni mesh. The bar scale is 10 μm. (b) Infrared transmission spectra of the same piece of Ni mesh in an FTIR microscope (top, red trace) and a standard benchtop FTIR (bottom, blue trace). Inset shows simple drawings of the basic optical schemes in the microscope and benchtop spectrometers.

RESULTS

The peak maxima were extracted from each transmission spectrum of Figure 3 and plotted versus φ in Figure 4. The peak maxima were found using the instrument's Perkin-Elmer commercial software. Each transmission spectrum was smoothed with the "Autosmooth" function employing a Savitzky−Golay approach with controls to prevent peak attenuation. Each smoothed spectrum then was multiplied by −1, added to 100% transmission, and converted to absorbance, which let the commercial software find the peaks with its absorption spectrum interpolation routine. The resonance peaks have been labeled with (i,j) values, and their dispersion was modeled using eq 2 as shown with solid lines in Figure 4. The model curves use $\theta_0 = 28.5°$, $n_{\text{eff}} = 1.040$, and an offset in φ of +5.0°. There is symmetry (predicted and evident) in the dispersion data about $\varphi = 45°$, and the offset of +5.0° gave the best overlap of the folded data. The aperture was positioned visually (not mechanically), so a small offset was reasonable. The model, with only two adjustable parameters, gives an excellent accounting of the dispersion of the strongest/main resonances, $(-1,-1)$ and $(-1,1)$. The value of θ_0 is right in the middle of the manufacturer's specified range and is reasonable, but depends on exactly where the aperture is placed in the instrument.

High symmetry spectra at $\varphi = 0°$ and 45° are shown in Figure 5 including the offset. At $\varphi = 0°$ (mesh holes aligned with *y*-axis), there is a strong (18.6% transmission) and narrow (fwhm = 95 cm^{-1}) peak at 826 cm^{-1}. This arises due to four different resonances assigned to *i,j* = (0,−1), (−1,−1), (0,1), and (−1,1), which nearly intersect at one point in φ-space. It has a mirror image at $\varphi = 90°$ for *i,j* = (−1,0), (−1,−1), (1,0), and (1,−1). The splitting at this point is a combination of front back coupling and interaction of different resonances. At $\varphi = 45°$ (mesh holes rotated by 45° in focal plane), there is a strong (17.4% transmission) peak at 1187 cm^{-1}, which arises due to the near intersection of eight different resonances with, *i,j* = (−1,1), (0,1), (1,−1), (1,0), (−2,0), (−2,−1), (−1,−2), and (0,−2) in φ-space. The momentum matching equation predicts that they would be degenerate at $\theta_0 = 27.7168°$ (at $n_{eff} = 1.040$), which is only 0.8° less than the best simulated value. These intersections at high symmetry places in φ-space are the reason that there are two major bumps in the transmission spectrum of the mesh without an aperture (Figure 1b, top). It is also very interesting that at $\varphi = 45°$, there is a fairly sharp (fwhm = 22 cm^{-1}) peak at 745 cm^{-1} of 6.0% transmission. This peak arises due to only one resonance, *i,j* = (−1,−1), and its width is likely limited by a range of angles associated with the width of the aperture (±2.2° about θ_0 and ±4.9° about φ). Sharp plasmonic resonances are much more useful than broad ones for detecting plasmonic shifts. When the aperture was narrowed to a width of 1.59 mm, the resonance was observed to have a fwhm of only 12 cm^{-1}, showing that the spread of angles was still the limiting effect. Unfortunately, the signal-to-noise was not very good because a smaller aperture uses an even smaller fraction of the microscope's intended light source.

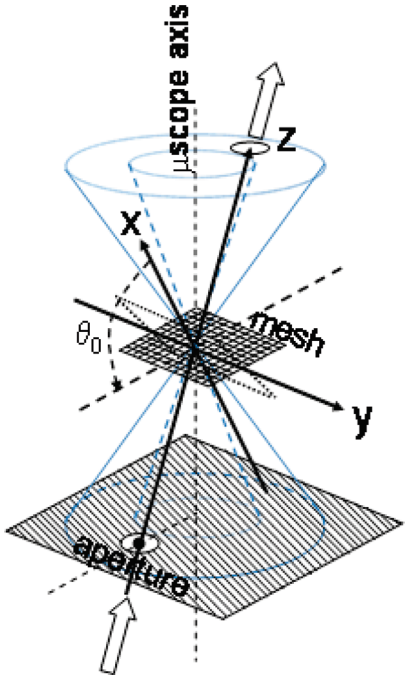

Figure 2. The coordinate system of a piece of mesh at the optical focus of a Cassegrain optical system in an FTIR microscope. An aperture (bottom) and the mesh (at the focal plane, middle) define the *z*-axis as the transmission axis. Letting the *y*-axis be within the mesh, the mesh is rotated by a fixed angle of $\theta_0 = \sim 28°$ about the *y*-axis until it is parallel with the ground and within the microscope's focal plane. The dispersion coordinate is rotation about the microscope axis to change φ at fixed θ.

CONCLUSION

The addition of an aperture greatly narrowed the resonances of the transmission spectrum of mesh in an FTIR microscope. The resonances change position upon rotation of the mesh in the focal plane of the microscope relative to the aperture's position; that is, they disperse in a manner that was quantitatively predicted with a momentum matching dispersion equation [eq 2]. This model fits the results very well and identifies the resonances. These results

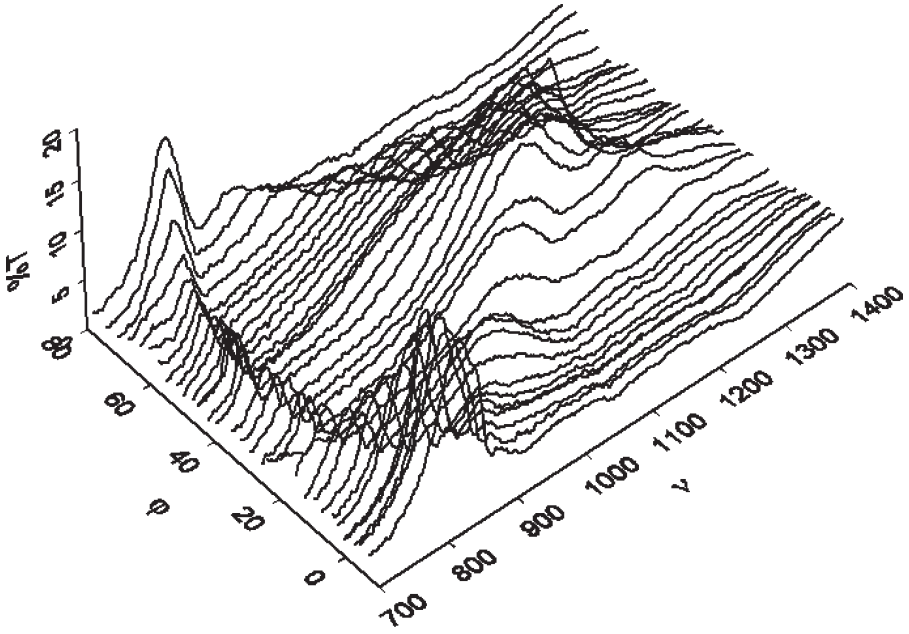

Figure 3. Transmission spectra of Ni mesh as a function of φ (rotation of the mesh within the focal plane relative to the position of the aperture). Note the definitive patterns of dispersion, that is, shifting of the transmission resonances.

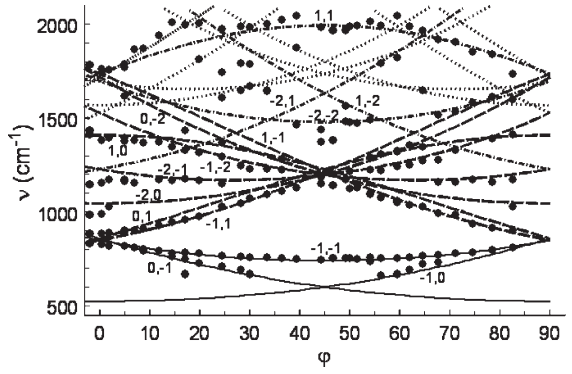

Figure 4. Dispersion plot of transmission resonance position versus the angle φ (rotation of the mesh within the microscope focal plane relative to the position of the aperture about the microscope's optical axis). The filled symbols are experimental peak positions of resonances as extracted from the data presented in Figure 3. The lines are given by the momentum matching eq 2 for different values of *i,j*. At $\varphi = 0°$, four different resonances [(0,−1), (−1,−1), (0,1), and (−1,1)] merge at ∼826 cm^{-1}, and at $\varphi = 45°$, eight different resonances [(0,1), (−1,1), (−2,0), (−2,−1), (1,0), (−1,−2), (0,−2), and (1,−1)] merge at ∼1187 cm^{-1}. The (−1,−1) and (1,1) resonances are particularly isolated from other resonances at a working range of φ about 45°.

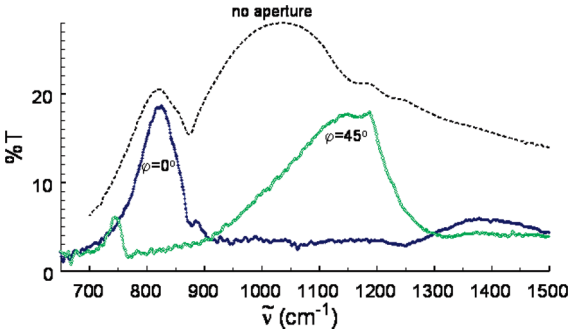

Figure 5. FTIR transmission spectra of Ni mesh at $\varphi = 0°$ and $\varphi = 45°$ using an aperture as compared to the same mesh without an aperture. The spectra at $\varphi = 0°$ and $\varphi = 45°$ are high symmetry places in φ-space that give rise with angle spreading to the two bumps in the microscope spectrum of Ni mesh without an aperture (dotted trace).

show that a nonpolarized, commercial IR microscope can be changed into a plasmonic imaging device by the simple addition of an aperture and mesh.

These results also help to explain the appearance of the microscope transmission spectrum without an aperture. The high symmetry overlapping resonances at $\varphi = 0°$ and 45° give rise to the two main peaks in the transmission spectrum of mesh without an aperture, allowing for averaging of dispersion over angles. There is no primary resonance at the benchtop position because there are no rays of perpendicular incidence with the microscope. Also, there is higher transmission in the microscope spectrum at higher wavenumbers because the microscope can collect higher order diffraction spots, whereas a benchtop instrument only collects the zero order spot.

The momentum matching model [eq 2] at $\varphi = 45°$ shows that only a small change in θ_0 from the best model value of 28.5° to 27.7168° is required to bring eight different resonances into degeneracy, a situation we call the "monster" SPP. Note that the

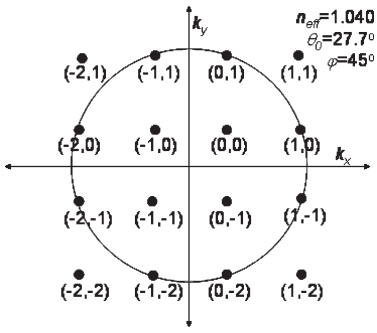

Figure 6. The conditions of tilting the mesh by $\theta_0 = 27.7°$ at $n_{eff} = 1.040$ and rotating by $\varphi = 45°$ shift the diffraction spots by 1/2 of a Brillouin zone in both the k_x and the k_y directions. Note the equidistant arrangement of the (0,1), (1,0), (−1,−1), (0,−2), (−1,−2), (−2,−1), (−2,0), and (−1,1) diffraction spots (as indicated with a circle) at this geometry. It is not a coincidence that these are the same labels of the resonances that contribute to the "monster plasmon". At the wavelength that corresponds to 1206 cm^{-1}, these spots (which are diffraction spots at shorter wavelengths) are deflected by 90°; that is, they are no longer transmitted, but trapped as evanescent waves along the surface of the mesh becoming the resonance.

exact angle for the monster SPP depends on the value of n_{eff}, which was modeled at 1.040. Only small changes in the optics or aperture positioning would be required to explore this region. An explanation for this resonance is offered in the k_y versus k_x plot of Figure 6, which is analogous to a diffraction pattern. The ideal arrangement (tilt of $\theta_0 = 27.7168°$ at $n_{eff} = 1.040$ and rotation about the microscope's optical axis of $\varphi = 45°$) shifts the diffraction spots by 1/2 a Brillouin zone in both the k_x and the k_y directions. As a result, the (0,1), (1,0), (−1,−1), (0,−2), (−1,−2), (−2,−1), (−2,0), and (−1,1) diffraction spots are equidistant from the origin; that is, they lie on a circle centered at the origin (see Figure 6). These diffraction spot labels are the same as those that label the "monster plasmon". At the wavelength that corresponds to 1206 cm^{-1}, these spots (which are diffraction spots at shorter wavelengths) are deflected by 90°; that is, they are no longer transmitted, but trapped as evanescent waves along the surface of the mesh becoming the resonance. It is also clear from the dispersion data that the degeneracy of the momentum matching equations will be lifted by the strong interaction of participating resonances.

The dispersion diagram of Figure 4 enables us to find regions of momentum space where resonances are isolated from other resonances. For instance, at $\varphi = 45°$, both the (−1,−1) and the (1,1) resonances are reasonably isolated. This may turn out to be important for the study of resonance properties, because most of the resonances we have studied to date are overlapped and strongly perturbed by interactions with other resonances. Finally, the *i,j* = (−1,−1) resonance is very narrow having a fwhm of only 22 cm^{-1}, which might prove useful with lifetime and single particle studies.

AUTHOR INFORMATION

Corresponding Author

*E-mail: coe.1@osu.edu.

ACKNOWLEDGMENT

We thank the National Science Foundation for support of this work under grant numbers CHE 0848486 and CHE 0639163.

REFERENCES

(1) Williams, S. M.; Stafford, A. D.; Rodriguez, K. R.; Rogers, T. M.; Coe, J. V. *J. Phys. Chem. B* **2003**, *107*, 11871–11879.

(2) Williams, S. M.; Rodriguez, K. R.; Teeters-Kennedy, S.; Shah, S.; Rogers, T. M.; Stafford, A. D.; Coe, J. V. *Nanotechnology* **2004**, *15*, S495–S503.

(3) Rodriguez, K. R.; Shah, S.; Williams, S. M.; Teeters-Kennedy, S.; Coe, J. V. *J. Chem. Phys.* **2004**, *121*, 8671–8675.

(4) Williams, S. M.; Rodriguez, K. R.; Teeters-Kennedy, S.; Stafford, A. D.; Bishop, S. R.; Lincoln, U. K.; Coe, J. V. *J. Phys. Chem. B* **2004**, *108*, 11833–11837.

(5) Teeters-Kennedy, S. M.; Rodriguez, K. R.; Rogers, T. M.; Zomchek, K. A.; Williams, S. M.; Sudnitsyn, A.; Carter, L.; Cherezov, V.; Caffrey, M.; Coe, J. V. *J. Phys. Chem. B* **2006**, *110*, 21719–21727.

(6) Coe, J. V.; Williams, S. M.; Rodriguez, K. R.; Teeters-Kennedy, S.; Sudnitsyn, A.; Hrovat, F. *Anal. Chem.* **2006**, *78*, 1384–1390.

(7) Coe, J. V.; Rodriguez, K. R.; Teeters-Kennedy, S.; Cilwa, K.; Heer, J.; Tian, H.; Williams, S. M. *J. Phys. Chem. C* **2007**, *111*, 17459–7472.

(8) Rodriguez, K. R.; Tian, H.; Heer, J. M.; Coe, J. V. *J. Phys. Chem. C* **2007**, *111*, 12106–12111.

(9) Rodriguez, K. R.; Tian, H.; Heer, J. M.; Teeters-Kennedy, S.; Coe, J. V. *J. Chem. Phys.* **2007**, 126.

(10) Coe, J. V.; Heer, J. M.; Teeters-Kennedy, S.; Tian, H.; Rodriguez, K. R. *Annu. Rev. Phys. Chem.* **2008**, *59*, 179–202.

(11) Cilwa, K. E.; Rodriguez, K. R.; Heer, J. M.; Malone, M. A.; Corwin, L. D.; Coe, J. V. *J. Chem. Phys.* **2009**, *131*, 061101.

(12) Heer, J.; Corwin, L.; Cilwa, K.; Malone, M. A.; Coe, J. V. *J. Phys. Chem. C* **2010**, *114*, 520–525.

(13) Malone, M. A.; Prakash, S.; Heer, J. M.; Corwin, L. D.; Cilwa, K. E.; Coe, J. V. *J. Chem. Phys.* **2010**, *133*, 185101.

(14) Ghaemi, H. F.; Thio, T.; Grupp, D. E.; Ebbesen, T. W.; Lezec, H. J. *Phys. Rev. B: Condens. Matter Mater. Phys.* **1998**, *58*, 6779–6782.

(15) Hendry, E.; Hibbins, A. P.; Sambles, J. R. *Phys. Rev. B* **2008**, *78*, 235426.

(16) Ming-Wei, T.; Tzu-Hung, C.; Hsu-Yu, C.; Si-Chen, L. *Appl. Phys. Lett.* **2006**, *88*, 213112.

(17) Ming-Wei, T.; Tzu-Hung, C.; Hsu-Yu, C.; Si-Chen, L. *Appl. Phys. Lett.* **2006**, *89*, 093102.

(18) Pelouard, J. L.; et al. *Appl. Phys. Lett.* **2008**, *92*, 011125.

(19) Williams, S. M.; Coe, J. V. *Plasmonics* **2006**, *1*, 87–93.

(20) De Abajo, F. J. G. *Rev. Mod. Phys.* **2007**, *79*, 1267.

(21) Garcia-Vidal, F. J.; Martin-Moreno, L.; Ebbesen, T. W.; Kuipers, L. *Rev. Mod. Phys.* **2010**, *82*, 729.

(22) Williams, S. M. Characteristics and Applications of the Infrared Enhanced Transmission of Metallic Subwavelength Arrays. Ph.D. Thesis, The Ohio State University, 2006.